

CHAPTER 5

RESULTS AND DISCUSSION (PART II):

LEAD TITANATE

In this chapter, the results are presented of the investigation of both powder and ceramic forms of lead titanate (PT). Phase formation-structure-processing relationships are brought out for this component, and discussed in terms of phase formation, morphology, particle size, densification, microstructure, dielectric properties and thermal expansion. Therefore, it is appropriate to focus initially on the synthesis of PT powders, before embarking on the fabrication of dense PT ceramics.

5.1 Lead Titanate Powders

TG-DTA curves recorded at a heating rate of 10 °C/min in air for an equimolar mixture of lead oxide and titanium oxide are shown in Fig. 5.1. It is demonstrated two distinct weight losses below 400 °C. The first weight loss occurs below 100 °C and the second one above 200 °C. In the temperature range from room temperature to ~ 150 °C, the sample shows exothermic peaks in the DTA curves at 120 °C, which are related to the first weight loss. These DTA peaks can be attributed to the decomposition of the organic species originating from the milling process [64]. Corresponding to the second fall in specimen weight, by increasing the temperature up to ~ 800 °C, the solid-state reaction between lead oxide and titanium oxide occurs. The broad exothermic characteristic present in all the DTA curves represents that reaction, which has a maximum at ~ 500-750 °C. No further significant weight loss was observed for temperatures above 500 °C in the TG curve, indicating that the

minimum firing temperature to form PbO-TiO_2 compounds is in good agreement with XRD results (Fig. 5.2) and those of previous authors [46,54].

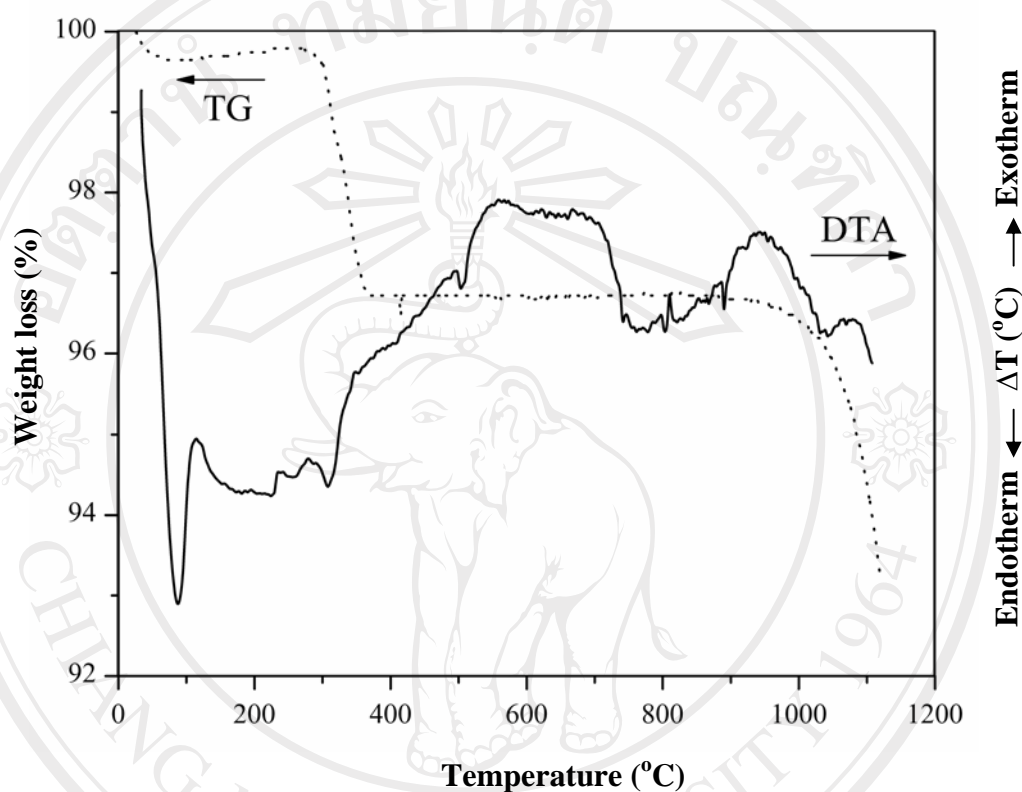


Fig. 5.1 TG-DTA curves for the mixture of PbO-TiO_2 powders.

All calcined powders, together with that of the starting powder mixtures were examined by XRD in order to investigate the phase development (Figs. 5.2-5.4). As shown in Fig. 5.2, for the uncalcined powder, only X-ray peaks of precursors PbO (\blacktriangledown) and TiO_2 (*) are present, indicating that no reaction was yet triggered during the vibro-milling process. However, after calcination at 500°C , it is seen that the perovskite-type PT becomes the predominant phase indicating that the reaction has occurred to a considerable extent. By increasing the calcination temperature from 550

to 650 °C, the single phase of perovskite PT (yield of 100% with in the limitations of the XRD technique) was obtained.

In general, the strongest reflections apparent in the majority of these XRD patterns indicate the formation of PT. These can be matched with JCPDS file number 6-452 for the tetragonal phase, in space group $P4/mmm$ with cell parameters $a = 3.90$ Å and $c = 4.15$ Å [171], consistent with other works [64,172].

Having established the optimum calcination temperature, alternative dwell times ranging from 1 to 4 h with constant heating/cooling rates of 20 °C/min were applied at 600 °C, as shown in Fig. 5.3. The appearance of PbO phase indicated that full crystallization has not occurred at relatively longer calcination times. This is probably due to the effectiveness of vibro-milling and a carefully optimised reaction. The observation that the soaking time effect may also play an important role in obtaining a single-phase perovskite product is also consistent with other similar systems [15,137].

Apart from the calcination temperature and soaking time, the effect of heating/cooling rates on the formation behaviour of PT was also investigated. Four heating/cooling rates (5, 10, 15 and 20 °C/min) were selected for calcination condition of 600 °C for 2 h (Fig. 5.4). In this connection, it is shown that the yield of PT phase did not vary significantly with heating/cooling rates, indicating that fast heating/cooling rates can leads to full crystallization of PT phase without time for the formation of pyrochlore phase or lead vaporization. The observation that faster heating/cooling rates are required for lead-based ferroelectrics is also consistent with other investigators [135,136].

Based on the TG-DTA and XRD data, it may be concluded that over a wide range of calcination conditions, single phase PbTiO_3 cannot be straightforwardly formed via a solid state mixed oxide synthetic route. The experimental work carried out here suggests that the optimal calcination conditions for single phase PbTiO_3 is 600°C for 2 h with heating/cooling rates as fast as $20^\circ\text{C}/\text{min}$ which is closed to that of Pillai and Ravindran [46]. However, the optimal firing temperatures found here are significantly lower than that reported by Jaffe *et al.* [15] and Shirane *et al.* [50] ($> 1000^\circ\text{C}$).

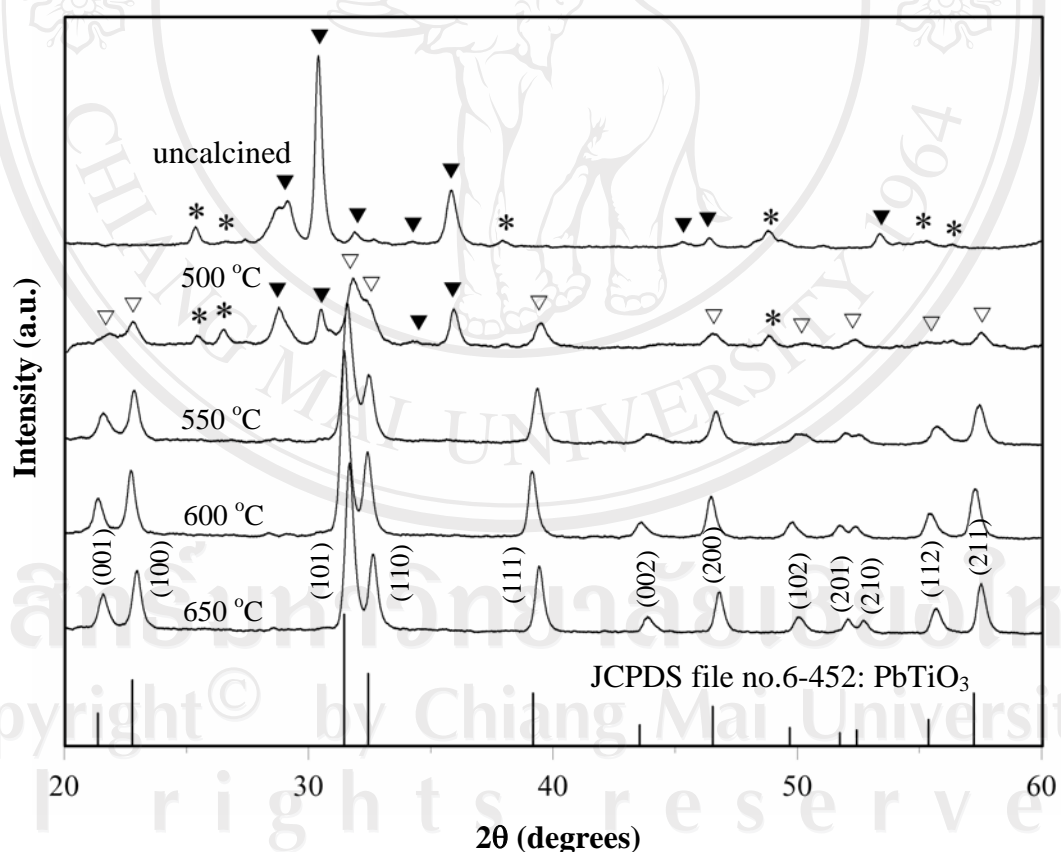


Fig. 5.2 XRD patterns of PT powders calcined at various temperatures for 2 h with heating/cooling rates of $20^\circ\text{C}/\text{min}$ (▼ PbO , * TiO_2 , ▽ PbTiO_3).

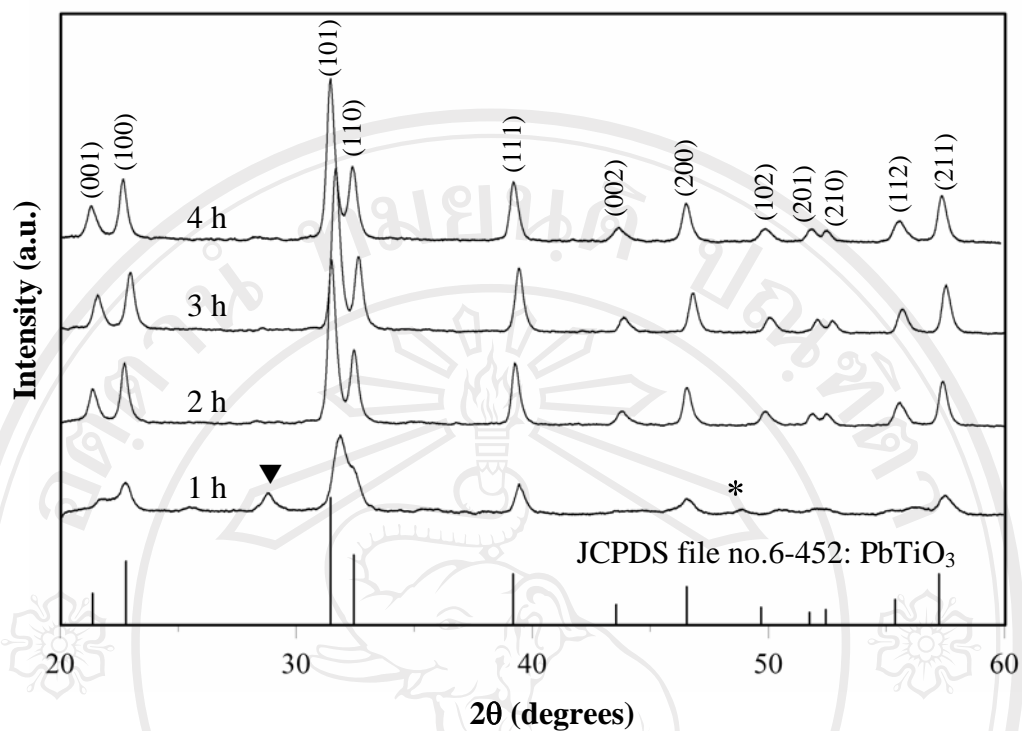


Fig. 5.3 XRD patterns of PT powders calcined at 600 °C with heating/cooling rates of 20 °C/min for various dwell times (▼ PbO and * TiO₂).

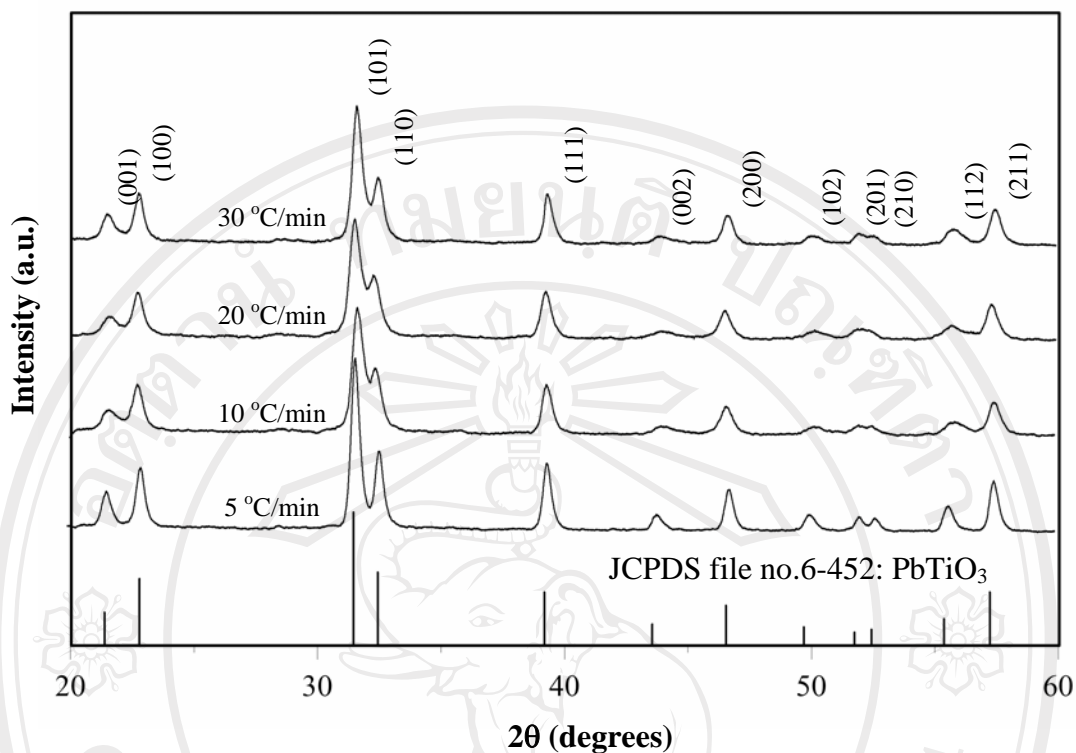


Fig. 5.4 XRD patterns of PT powders calcined at 600 °C for 2 h with various heating/cooling rates.

Table 5.1 Calculated PT phase as a function of calcination conditions.

Temperature (°C)	Dwell time (h)	Heating/cooling rates (°C/min)	Qualitative concentration of PT phase* (wt%)
500	2	20	-
550	2	20	100
600	1	20	-
600	2	5	100
600	2	10	100
600	2	20	100
600	2	30	100
600	3	20	100
650	4	20	100

* The estimated precision of the concentrations for the two phases is $\pm 0.1\%$.

- PbTiO_3 , PbO and TiO_2 phases were found and Eq. (3.5) is not valid.

SEM micrographs of the PT powders calcined at 550 and 600 °C are shown in Fig. 5.5 (a) and (b), respectively. It is seen that all powders seem to have similar morphology. In general, the particles are agglomerated and basically irregular in shape with a substantial variation in particle size, particularly in samples calcined at high temperatures. This structure is similar to that of PT powders synthesized by previous researchers [64,172]. The range of particle diameter was found to be about 0.1-0.2 μm and 0.1-0.25 μm for the samples calcined at 550 and 600 °C for 2 h,

respectively. The results indicate that averaged particle size and degree of agglomeration tend to increase with calcination temperature. In the next sections, PT powders calcined at 600 °C for 2 h were used for the fabrication of PT ceramics

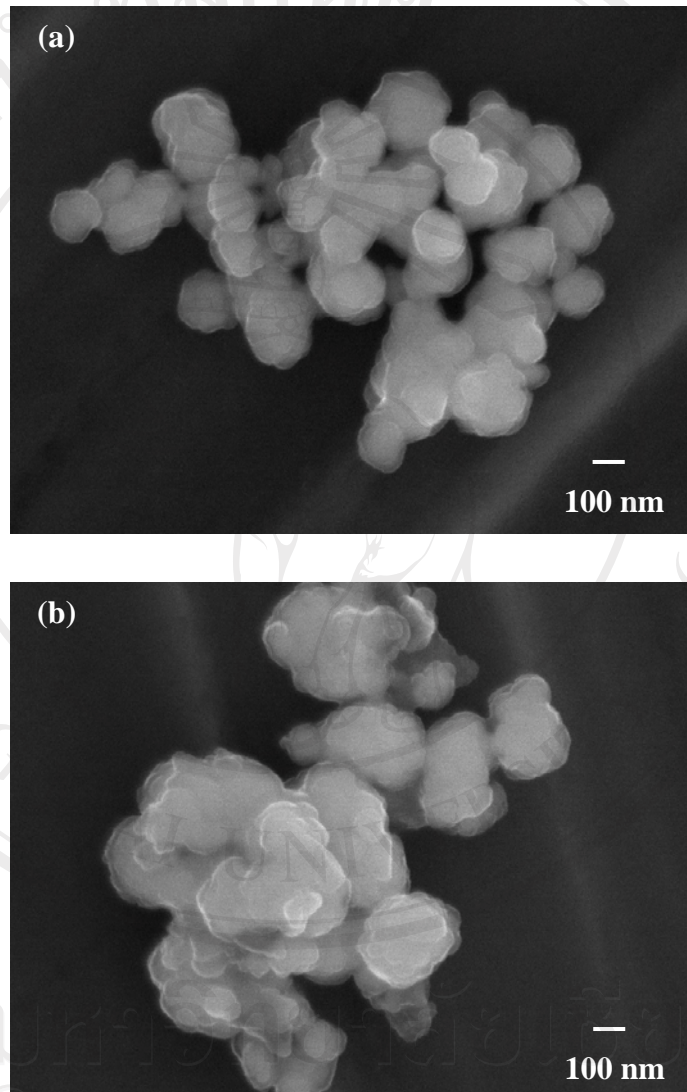


Fig. 5.5 SEM micrographs of the PT powders calcined at (a) 550 °C and (b) 600 °C, for 2 h with heating/cooling rates of 20 °C/min.

5.2 Lead Titanate Ceramics

In this section, attention is given to the chemical composition, densification, microstructure, thermal expansion and dielectric properties of single- and two-stage sintered PT ceramics. The optimum sintering temperature was determined by monitoring the bulk densities obtained for a dwell time of 2 h with heating/cooling rates of 1 °C/min at the range of temperature between 1150 °C and 1250 °C for the single-stage sintered samples. Three sets of the first sintering temperature (T_1) were assigned for the two-stage sintering case: 700, 800 and 900 °C. Variation of the second sintering temperature (T_2) between 1000 °C and 1250 °C was carried out for each case.

X-ray diffraction patterns of the PT ceramics sintered at various conditions are displayed in Figs. 5.6 and 5.7, indicating the formation of both perovskite and impurity phases in each case. The strongest reflections in the majority of all XRD traces indicate the formation of the PT perovskite phase, which could be matched with JCPDS file no. 6-452, in agreement with other works [79,81]. To a first approximation, this major phase has a tetragonal perovskite-type structure in space group $P4/mmm$ (no. 123) with cell parameters $a = 3.90 \text{ \AA}$ and $c = 4.15 \text{ \AA}$ [171]. For the singly sintered PT ceramics, additional weak reflections are found in the samples sintered above 1175 °C (marked by ▼ in Fig. 5.6), which correlate to the starting precursor PbO (JCPDS file no. 77-1971) [173]. This observation could be attributed mainly to the poor mixing of the employed powders derived from the ball-milling technique. The relative amounts of perovskite and minor phase present in each sintered ceramic were calculated from Eq. 3.9 (see section 3.2.2) (numerical data are presented in Tables 5.2 and 5.3).

More interestingly, a single phase of perovskite PT is found in all the doubly sintered samples (Fig. 5.7), in contrast to the observations for the singly sintered samples. No evidence of pyrochlore phase of PbTi_3O_7 composition earlier reported by Udornporn *et al.* and Tartaj *et al.* [64,174] was found, nor was there any evidence of other second phases [175] being present. This could be due to the lower firing temperature of the doubly sintered samples as compared to the singly sintered ceramics, leading to a smaller degree of lead losses and consequently avoiding the pyrochlore formation, while a sufficient amount of energy required for ceramic densification still to be reached was provided by the longer holding time, in agreement with other works [4,176]. However, many other factors come into play, e.g. homogeneity of materials, reactivity of starting powders and processing variables. These XRD results clearly show that, in general, the different processing methods used for preparing PT ceramics gave rise to a different phase formation in the sintered materials. The absence of minor phase in doubly sintered samples was related to the more reactive process used [4].

Table 5.2 Physical properties of singly sintered PT ceramics.

Sintering temperature (°C)	Perovskite phase (%)	Tetragonality (c/a)	Relative density (%)	Grain size range (mean)* (μm)
1150	100	1.064	87	2.5-15.0 (6.5)
1175	100	1.064	89	8.0-26.5 (13)
1200	99.3	1.063	92	12.0-40.0 (29)
1225	90.1	1.063	94	20.0-65.0 (36)
1250	89.2	1.063	93	41.0-83.0 (52)

* The estimated precision of the grain size is $\pm 10\%$.

Table 5.3 Physical properties of doubly sintered PT ceramics.

T_1 (°C)	T_2 (°C)	Perovskite phase (%)	Tetragonality (c/a)	Relative density (%)	Grain size range (mean)* (μm)
700	1000	-	-	-	-
700	1050	-	-	-	-
700	1100	100	1.058	96	0.3-0.5 (0.3)
700	1150	100	1.060	96	0.3-1.2 (0.8)
700	1200	100	1.062	96	0.4-1.7 (1.3)
700	1250	-	-	-	-
800	1000	-	-	-	-
800	1050	100	1.064	95	1.0-2.2 (1.6)
800	1100	100	1.061	96	0.5-3.3 (1.9)
800	1150	100	1.060	96	1.0-2.7 (1.8)
800	1200	100	1.062	96	0.6-1.7 (1.2)
800	1250	-	-	-	-
900	1000	-	-	-	-
900	1050	100	1.060	96	0.4-2.2 (1.2)
900	1100	100	1.060	96	0.7-1.5 (1.1)
900	1150	100	1.057	96	0.6-1.9 (0.8)
900	1200	100	1.061	97	1.0-2.2 (1.5)
900	1250	100	-	-	-

* The estimated precision of the grain size is $\pm 10\%$.

- Data are not available because the samples were too fragile for the measurements.

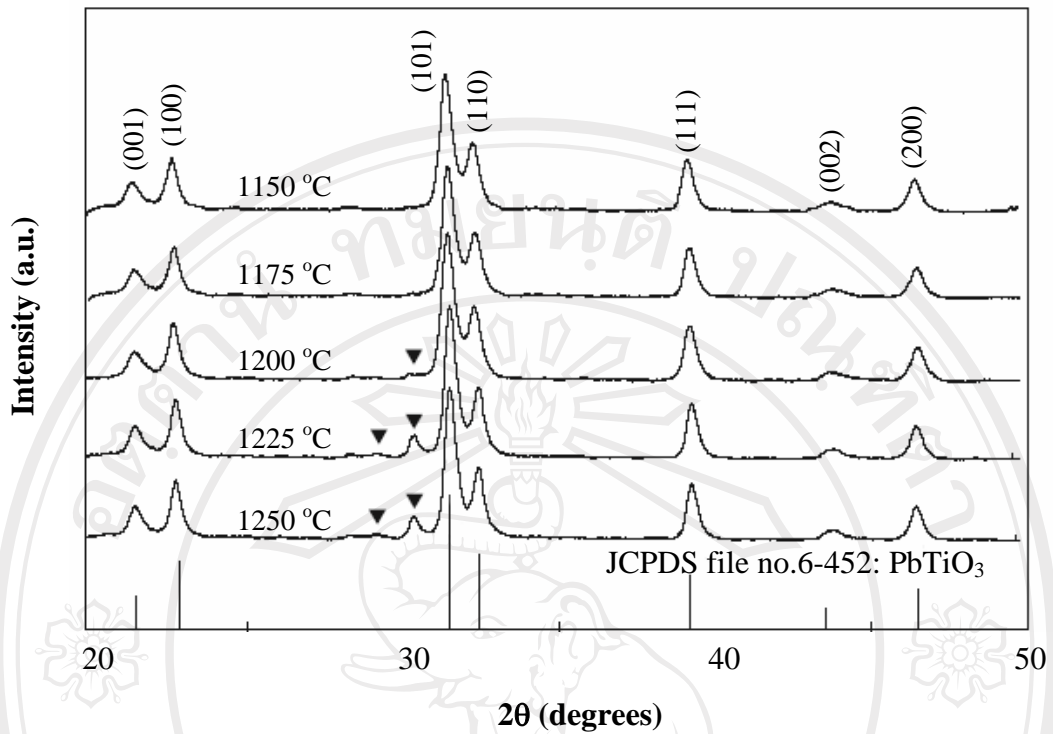


Fig. 5.6 XRD patterns of PT ceramics singly sintered at various temperatures (▼ PbO).

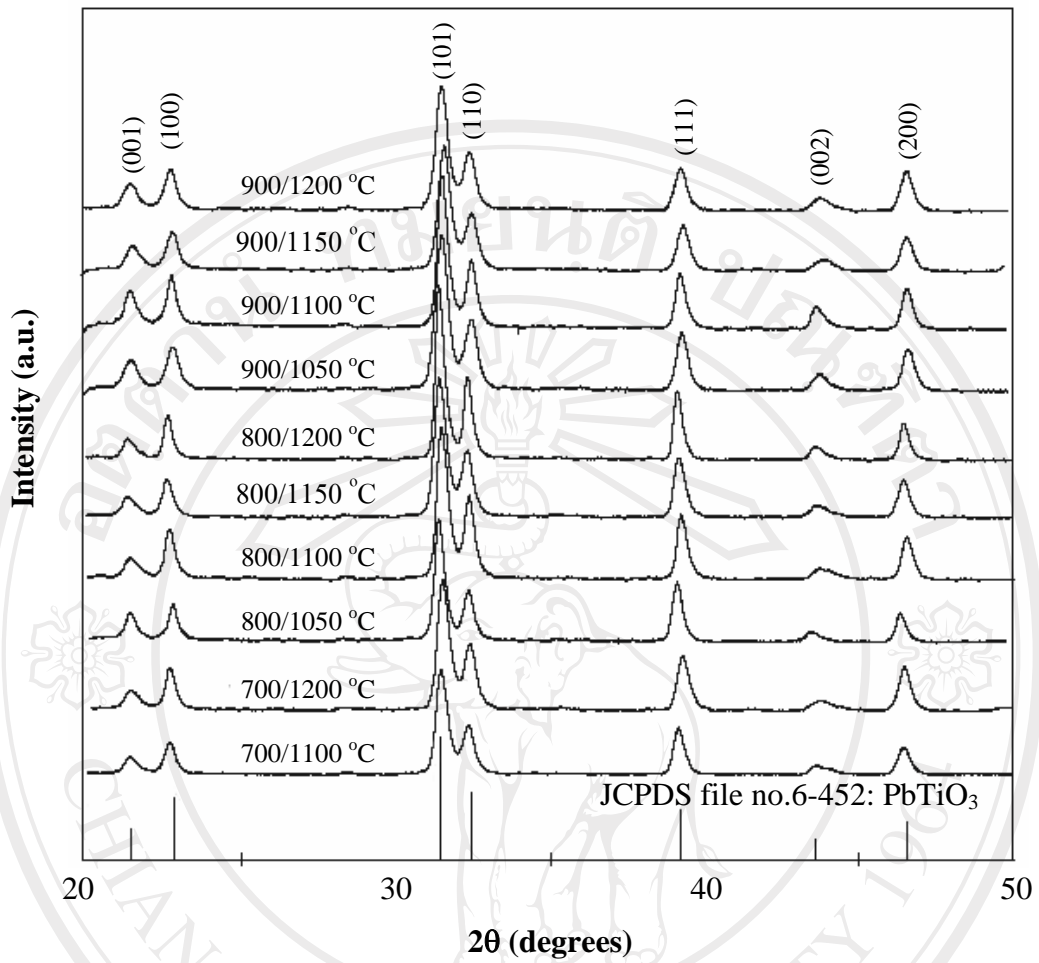


Fig. 5.7 XRD patterns of PT ceramics doubly sintered at various conditions, with the first sintering temperature (T_1) at 700, 800 and 900 °C.

Tables 5.2 and 5.3 also present the tetragonality factor (c/a), relative density and average grain size of singly and doubly sintered samples, respectively. Generally, it is evident that as the sintering temperature increases, the density of almost all the samples increases. However, it can be seen that the sintering behavior of singly and doubly sintered PT ceramics was dissimilar. Doubly sintered ceramics reached a maximum density of $\sim 97\%$ at $900/1150\text{ }^\circ\text{C}$ or $900/1200\text{ }^\circ\text{C}$. On the other hand, singly sintered samples exhibit less densification, and a temperature of $1225\text{ }^\circ\text{C}$ was required to reach a densification level of $\sim 94\%$. The densification of all materials slightly decreased at temperatures higher than those of the maximum density, accompanied by a significant increase of weight loss ($\sim 2\text{-}5\%$). By comparison with singly sintered PT ceramics, lower values of tetragonality (c/a) are found in all doubly sintered cases, indicating lower internal stress in these sintered samples.

The microstructural features of PT samples singly sintered at 1150 and $1225\text{ }^\circ\text{C}$ for 2 h with heating/cooling rates of $1\text{ }^\circ\text{C}/\text{min}$ are shown in Fig. 5.8. It was found that the samples subjected to low sintering temperature, e.g. $1150\text{ }^\circ\text{C}$, eventually burst into pieces because of the internal anisotropic stress caused by the phase transition in the ceramics, as can be confirmed by the SEM images showing a loose formation of large grains (Fig. 5.8 (a)), in agreement with high values of c/a given in Table 5.2. Additionally, average grain sizes were found to increase with the sintering temperature. For higher-temperature treatments, a pronounced second phase is segregated at the grain boundaries. The EDX spectra indicated that there was more Pb and less Ti in the bright region ($[\text{Pb}] : [\text{Ti}] \sim 4 : 1\text{ at.}\%$) than in the dark region ($[\text{Pb}] : [\text{Ti}] \sim 1 : 1\text{ at.}\%$), as shown in Fig. 5.8(b). The observation of these (second-phase)

layers could be attributed to a liquid-phase formation during the sintering process as proposed by many researchers [25,115].

Representative microstructures for doubly sintered PT ceramics are given in Fig. 5.9. The first sintering temperature was designed at 700, 800 and 900 °C, for constant dwell time and heating/cooling rates of 2 h and 1 °C/min at each stage, while the second sintering temperature was varied from 1100 °C to 1200 °C. It is seen that a uniform grain shape of typical perovskite ceramics [77,176] is observed, with sizes in the range of 0.4-2.0 μm. It should be noted that the average grain size of the doubly sintered PT ceramics is < 2.0 μm, which is less than the critical value of 3 μm reported by several workers [27,79]. Here, it is believed that smaller grains with random orientations result in lower internal stress in sintered samples because they compensate the anisotropy of thermal expansion coefficients.

By comparison with singly sintered PT ceramics, almost clean microstructures with high uniformity, denser angular grain packing and more homogeneity are generally observed in doubly sintered PT samples. These microstructures are typical of a solid-state sintering mechanism. In the present study (Fig. 5.9 and Table 5.3), the microstructural features of the doubly sintered PT ceramics with various second sintering temperatures ranging from 1050 to 1200 °C are not significantly different.

However, it should be noted that higher angular grains were evidenced for higher second sintering temperature (see Fig. 5.9 (b), (d) and (f)). The observation that the sintering temperature effect may also play an important role in obtaining a high angularity in the grains of perovskite ceramics is also consistent with other similar systems [177]. Moreover, an abnormal grain growth probably due to the inhibition of the normal grain growth mechanism during the double sintering process [4] was also

found in some samples, as shown in Fig. 5.9 (c). It is also of interest to point out that evidence has been found for the existence of microcracks (arrowed) along the grain boundaries of the samples sintered at lower second sintering temperatures (Fig. 5.9 (c) and (e)), in agreement with other works [28,77].

Interestingly, only the samples sintered at 700/1100-1200 °C, 800/1050-1200 °C or 900/1050-1200 °C with the highest relative density and smallest average grain size of about 95%-97% and 0.3-1.9 μm , respectively, remained unbroken. It may be simply assumed that the ceramics consisting of very fine grains have less elastic strain energy than the ceramics with significantly large grains (Tables 5.2 and 5.3). Consequently, the experimental work carried out here suggests that the optimum conditions for forming the highly dense PT ceramics in this work are double sintering temperatures at 700-900/1100-1200 °C, 2 h dwell time and 1 °C/min heating/cooling rates. The different microstructure evolution of PT ceramics confirms the importance of the processing method. More importantly, considered from the perovskite content and microstructure of PT ceramics sintered by two different methods, the doubly sintered method was clearly preferable for obtaining dense perovskite PT ceramics.

The following discussion of the dielectric properties of the PT ceramics obtained in this study would further support the advantage of the double sintering method.

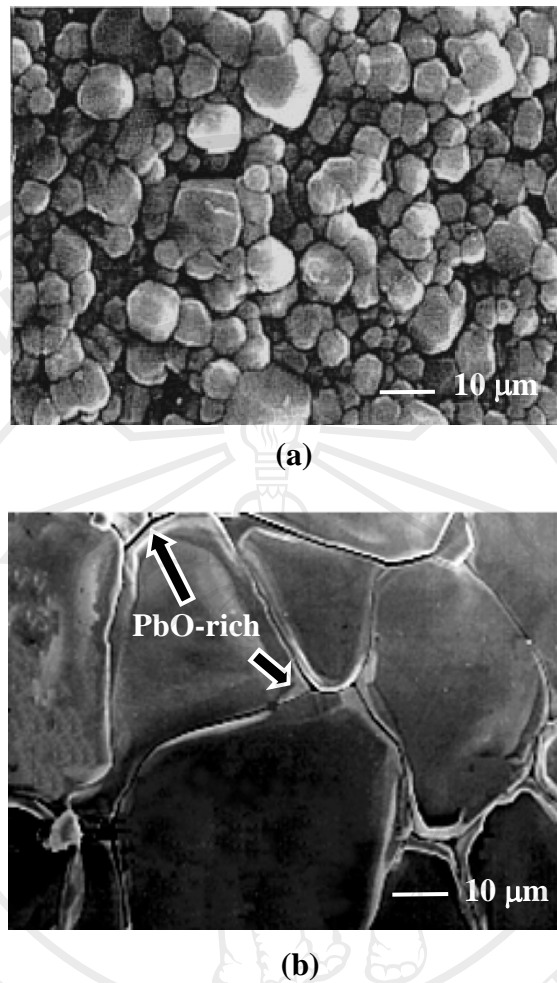


Fig. 5.8 SEM micrographs of PT ceramics singly sintered at (a) 1150 and (b) 1225 °C.

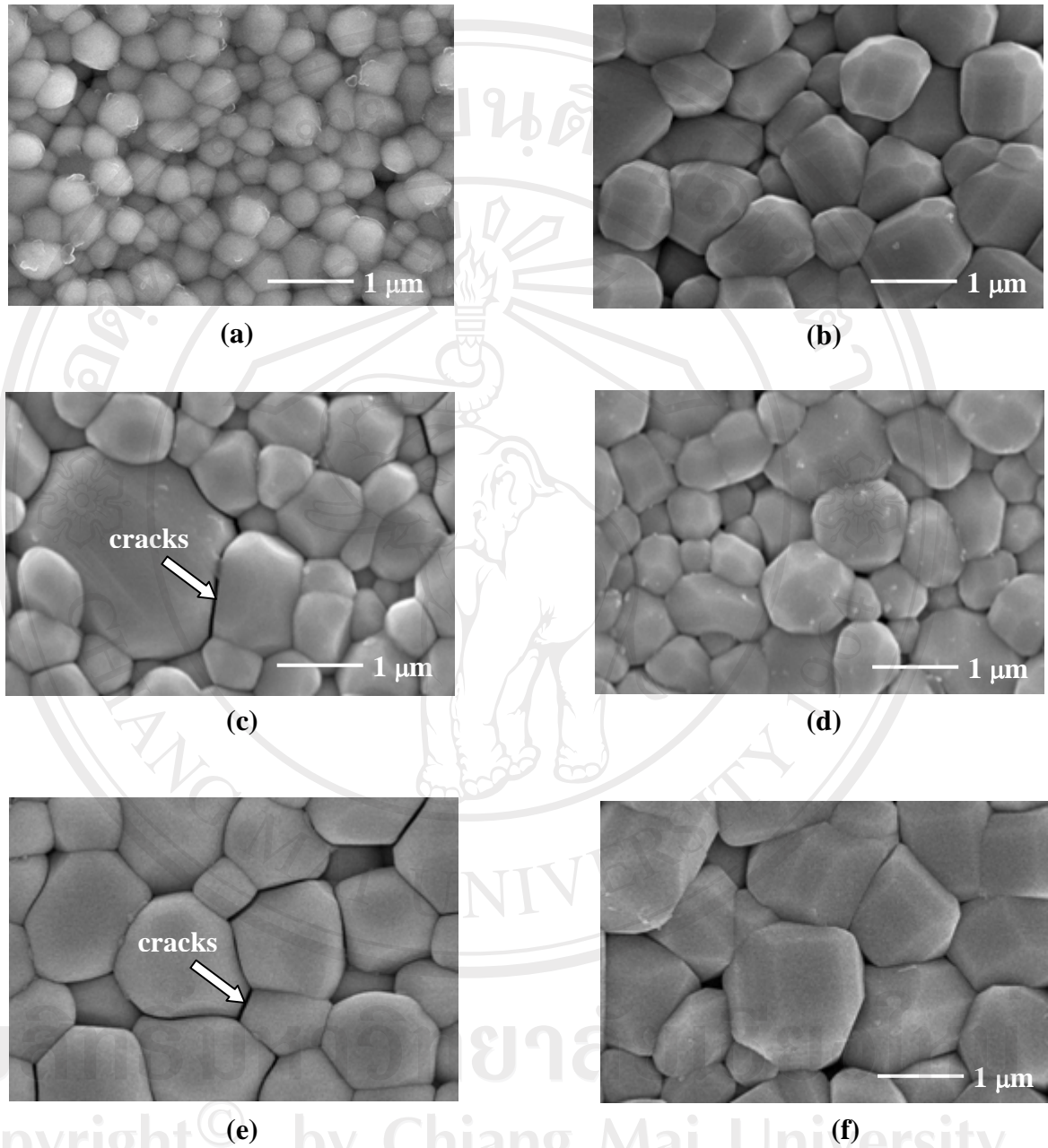


Fig. 5.9 SEM micrographs of PT ceramics doubly sintered at (a) 700/1100 (b) 700/1200 (c) 800/1100 (d) 800/1200 (e) 900/1100 and (f) 900/1200 °C.

The dielectric properties of the PT samples sintered with different techniques are also compared in Table 5.4, as well as in Figs. 5.10-5.13. The Curie temperatures are about the same for all samples measured, whilst the dielectric properties of both sets of the sintered PT ceramics seem to be different. As listed in Table 5.4, the room-temperature dielectric properties of the two sets of ceramics are not significantly different. The values of dielectric constant in the order of 200 are slightly higher than those reported earlier [77,177]. However, the high-temperature dielectric properties of the doubly sintered PT samples are noticeably higher than those of the singly sintered PT samples. As mentioned earlier, the reason for this is the high amount of secondary phase present in the singly sintered PT ceramics. In addition, a PbO-rich phase (as observed in Fig. 5.8 (b)), with low dielectric constant, might be forming a continuous layer between grains and hence de-creasing the dielectric constant of the singly sintered PT ceramics [41,81,116]. The secondary phases in singly sintered PT are interconnected at grain boundaries and, as suggested by Wang and Schulze [81], exert more influence on the dielectric properties than when they are isolated. It should also be noted that in singly sintered specimens the grain boundaries are mostly PbO-rich, while in doubly sintered specimens the grain boundaries are mainly PT with Pb/Ti ratio very close to 1. Although the number of grain boundaries increases in the doubly sintered ceramic, the improved properties are a result of a more chemical homogeneity of the microstructure in the doubly sintered ceramics. Therefore, in this study, it could be stated that the number of grain boundaries is not the main controlling factor for the properties in the doubly sintered ceramics, but the properties are rather dictated by the chemical composition of the grain boundaries.

Grain sizes also play a role in the difference in the dielectric properties, especially the dielectric constant. As clearly seen in Tables 5.2 and 5.3 (as well as Figs. 5.8 and 5.9), the larger grain size in the singly sintered ceramics would lead to lower dielectric constant than that of the doubly sintered ceramics. This relation is well established in several ceramic perovskite systems, e.g. BaTiO₃ [177], PZT (Pb(Zr_{1/2}Ti_{1/2})O₃) [178], PMN [35] and PFN [176].

The different microstructure and the different amount of secondary phases present in singly and doubly sintered PT ceramics strongly influence the dielectric properties of these materials, leading to superior electrical behavior in doubly sintered PT ceramics. Moreover, this study demonstrated that the dielectric properties of PT ceramics are also influenced by microstructural features, especially the phase compositions at grain boundaries, microcracks and the densification mechanism rather than by only pyrochlore phase or by grain size itself.

Although a disadvantage of the proposed two-stage sintering method is a greater time requirement, the significant reduction in firing temperature is a positive development, particularly with regard to the drive towards electrodes of lower cost [1,15]. In general, these PT ceramics exhibit complex microstructures which are a result of variation in grain size and orientation, variation in chemical homogeneity, and the presence and distribution of additional minor phase, pores and (micro)cracks. These factors, which are strongly influenced by the sintering conditions, have an important effect on the dielectric properties of materials and their reproducibility.

Table 5.4 Dielectric properties (at 1 MHz) of PT ceramics sintered at various conditions

Dielectric properties (1 MHz)	Sintering temperature (°C for 2 h)			
	Single	Double (T_1/T_2)		
		700/1200	800/1200	900/1200
ϵ_r (25 °C)	243	209	255	209
$\tan \delta$ (25 °C)	0.01	0.05	0.03	0.03
$\epsilon_{r, \max}$	7680	8993	8322	8198
$\tan \delta_{\max}$	1.07	1.00	1.10	0.95
T_C	482	484	484	484

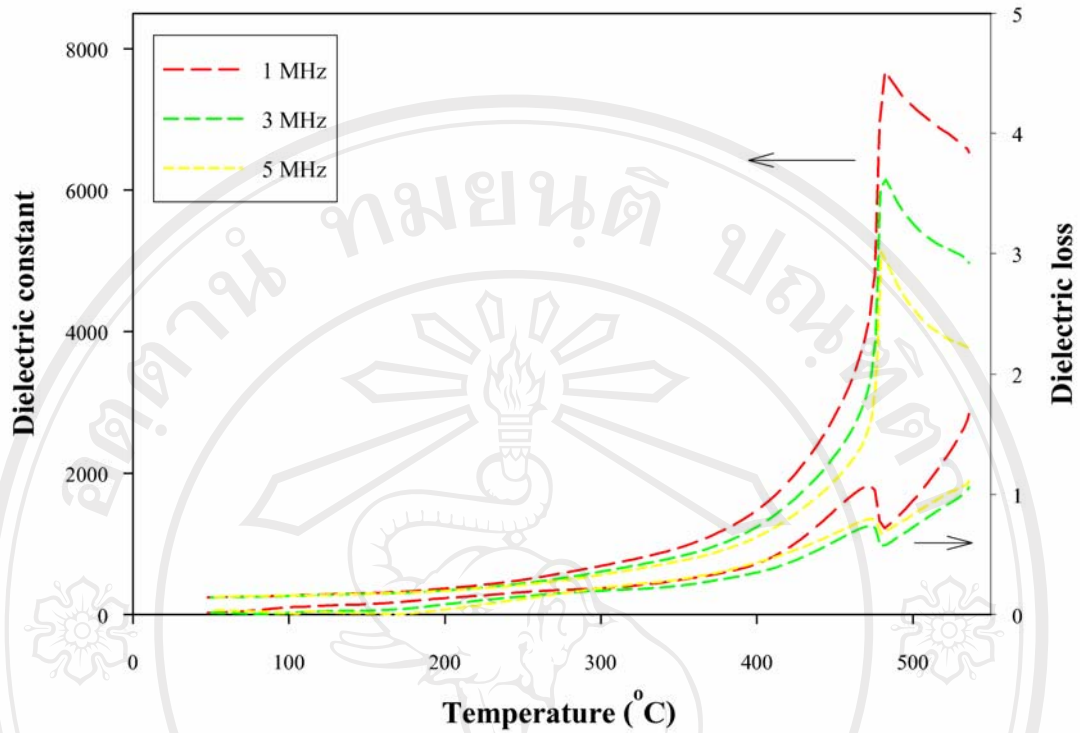


Fig. 5.10 Variation with temperature of dielectric constant and dielectric loss at various frequencies for singly sintered PT ceramic.

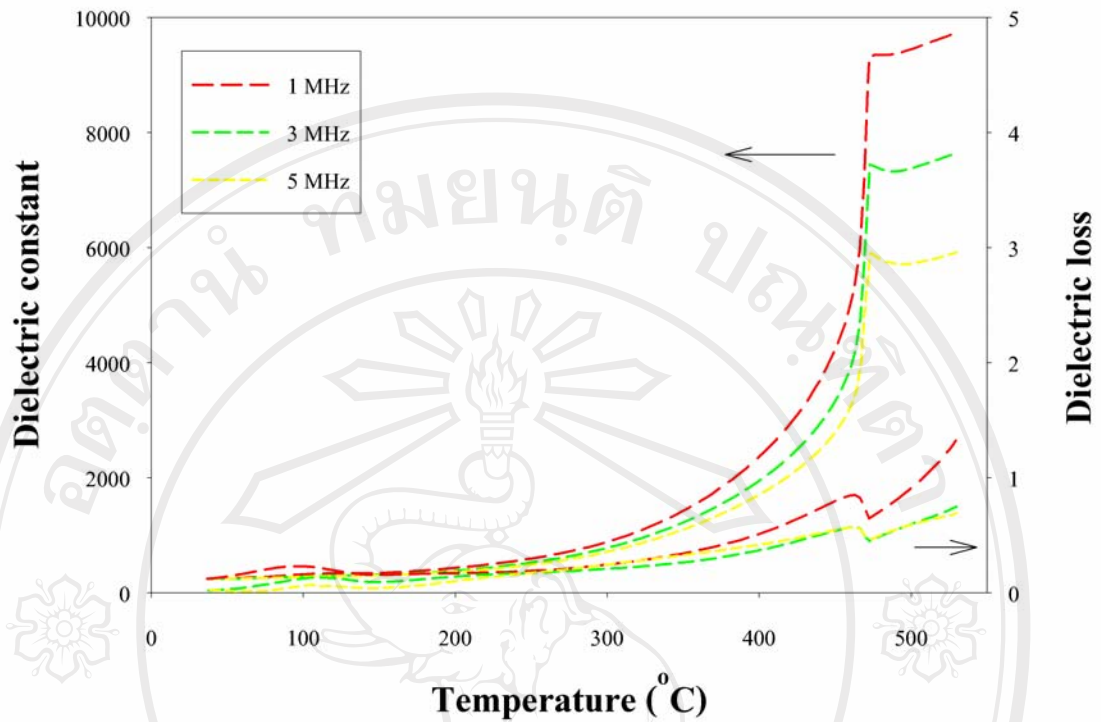


Fig. 5.11 Variation with temperature of dielectric constant and dielectric loss at various frequencies for PT ceramic sintered at 700/1200 °C.

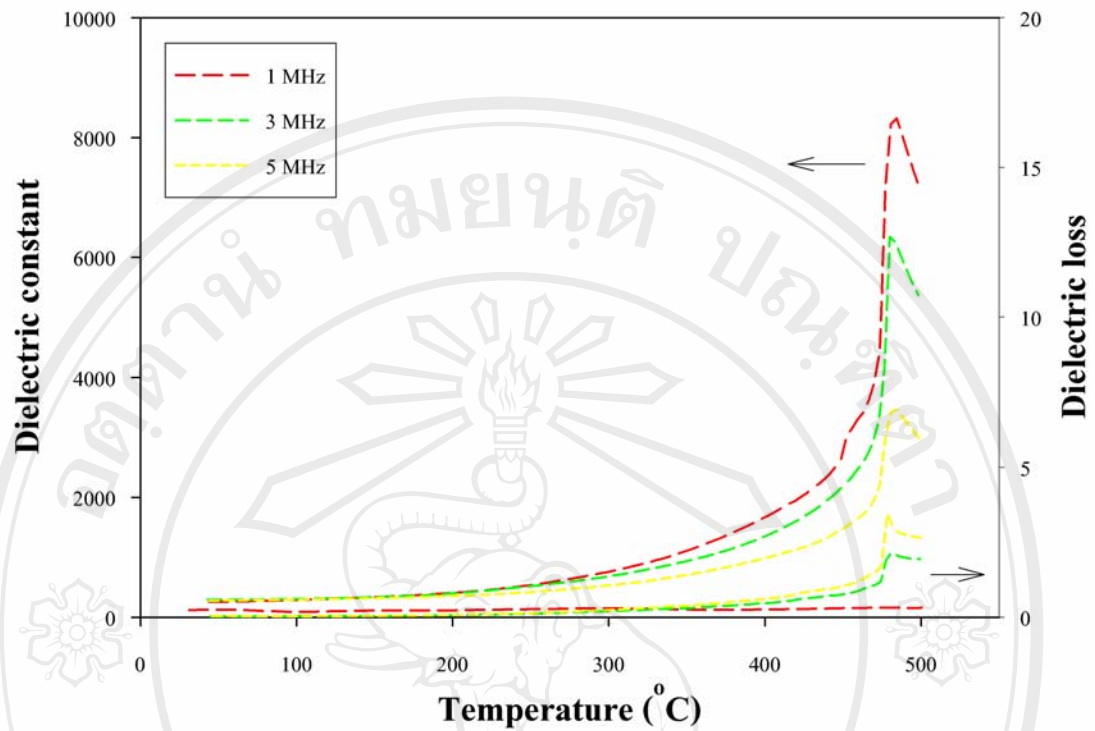


Fig. 5.12 Variation with temperature of dielectric constant and dielectric loss at various frequencies for PT ceramic sintered at 800/1200 °C.

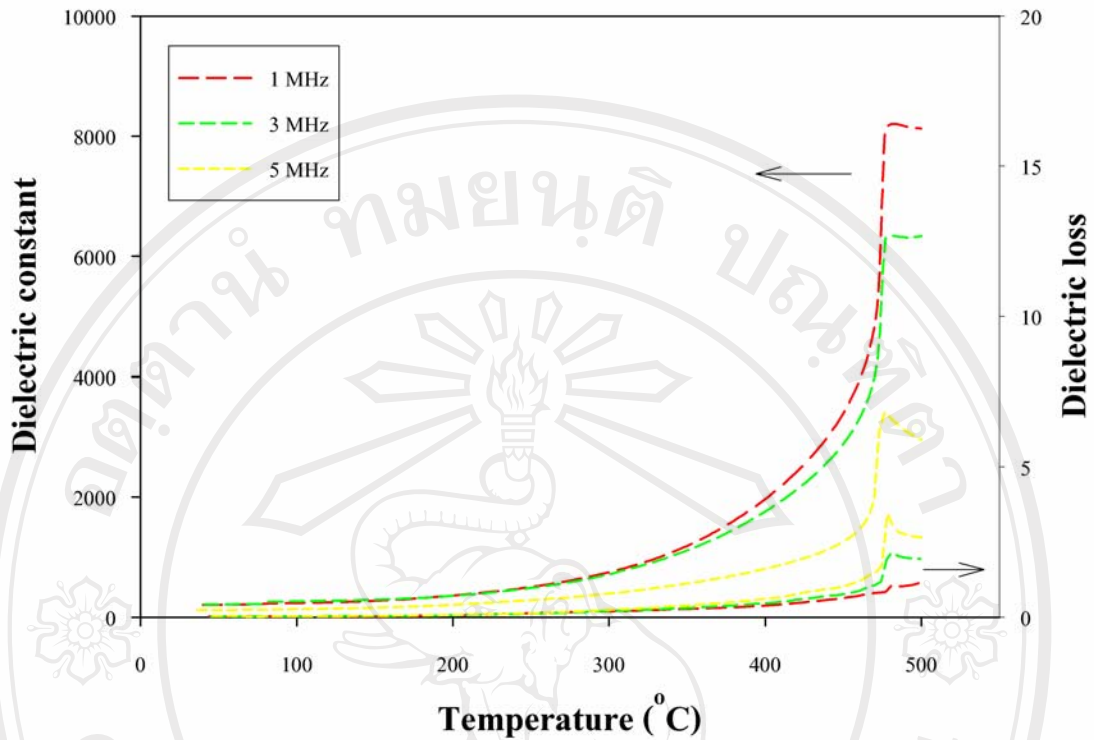


Fig. 5.13 Variation with temperature of dielectric constant and dielectric loss at various frequencies for PT ceramic sintered at 900/1200 °C.

The results of the thermal expansion properties for doubly sintered PT ceramics, shown in Fig. 5.14-5.16, indicate that the respective paraelectric-ferroelectric phase transition occur at around 515 °C for 700/1200 °C PT, at 490 °C for 800/1200 °C PT and at 486 °C for 900/1200 °C PT samples. The thermal expansion coefficients change sharply at the T_C , as determined from heating of three unpoled samples and the values are $-64 \times 10^{-6}/^{\circ}\text{C}$, $-70 \times 10^{-6}/^{\circ}\text{C}$ and $-83 \times 10^{-6}/^{\circ}\text{C}$, respectively. The phase transition temperature values are slightly different in the three samples. However, they are in good agreement with the published [179,180] values. Furthermore, the thermal expansion (or strain) in these samples is linear at temperatures above $T_C \approx 490$ °C. At temperatures below Curie temperature, these linear thermal expansions are superimposed by a ceramic's spontaneous polarization. Following a thermal cycle, an unpoled ceramic will obviously return very much to the state of distortion it had before the cycle except for 700/1200 °C PT ceramic. The thermal expansion could not be highly reproducible, that may be related to the average grain sizes which are smaller than that observed in the other two samples.

Effects of poling on thermal expansion properties of PT ceramic sintered at 900/1200 °C, was also examined. Bar shaped PT ceramic sample was poled perpendicular and parallel to the length direction (and in reference to the measuring direction) with an applied electric field in an oil bath for 15 minutes at 120 °C. Figs. 5.17 and 5.18 show the expansion parallel and perpendicular to the poling direction, respectively. The poled sample was depolarized during a measurement cycle, which makes the determination of the change in deformation caused by the poling possible. The reduction of the spontaneous strain for sample poled both perpendicular and parallel direction are compared to unpoled sample and can be seen in Fig. 5.19. It is

also desirable to understand the behavior of spontaneous strain in poled ceramic. The contribution of the spontaneous polarization to strain is due to the electrostrictive coupling. By extrapolating structural strain to the ferroelectric region, the contribution of ferroelectric transition to the spontaneous strain can be deduced. Other reason which is possible, is that the sample has built in surface charge or “locking field” on the both surfaces of poled sample. These surfaces might be affected by opposite charges and it can reduce or change the strain values of ceramic sample. For perpendicular to the poling direction, the effect of poling has no appreciable effects on expansion of sample. Moreover, it can be noted that the transition temperature value of both perpendicular and parallel poled samples were comparatively decreased from Curie point of the unpoled sample. And the poling has no effect in the paraelectric state for both poled states PT sample.

It is also clear that there are minimums or no differences in the values of thermal expansion coefficients during heating and cooling cycles which suggests that even going through the phase transition of PT, no apparent cracks developed in the samples. The data is also suggestive of the useful approach of two stage sintering adopted in the current synthesis of the samples. The thermal expansion data can further be expanded to estimate the P_S values, T_C and nature of transition.

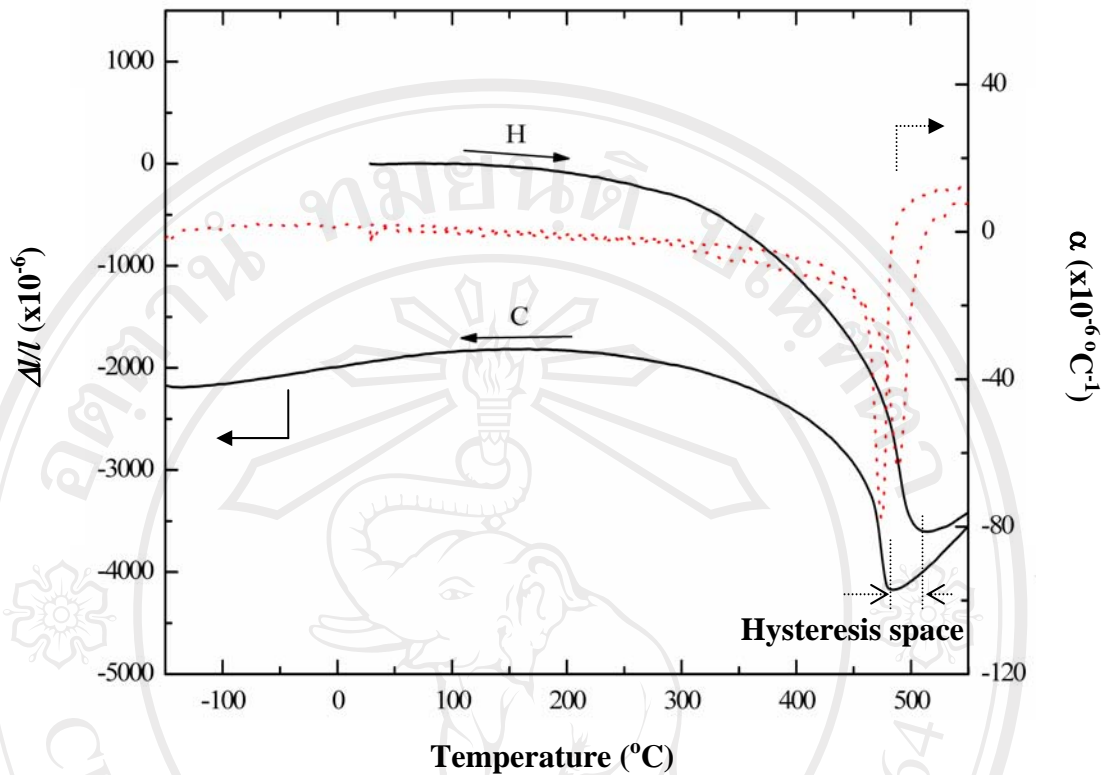


Fig. 5.14 Thermal expansion ($\Delta l/l$) and thermal expansion coefficient (α) of unpoled PT ceramic sintered by two stage process at 700/1200 °C as a function of temperature (H = heating cycle and C = cooling cycle).

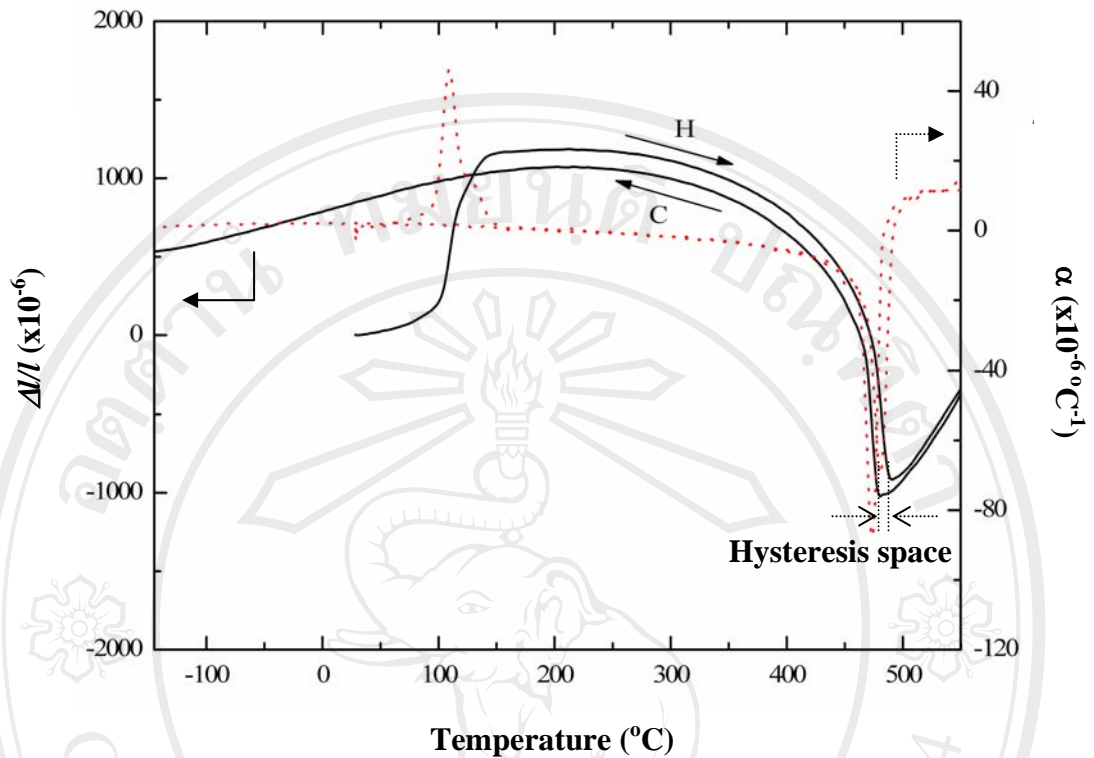


Fig. 5.15 Thermal expansion ($\Delta l/l$) and thermal expansion coefficient (α) of unpoled PT ceramic sintered by two stage process at 800/1200 °C as a function of temperature (H = heating cycle and C = cooling cycle).

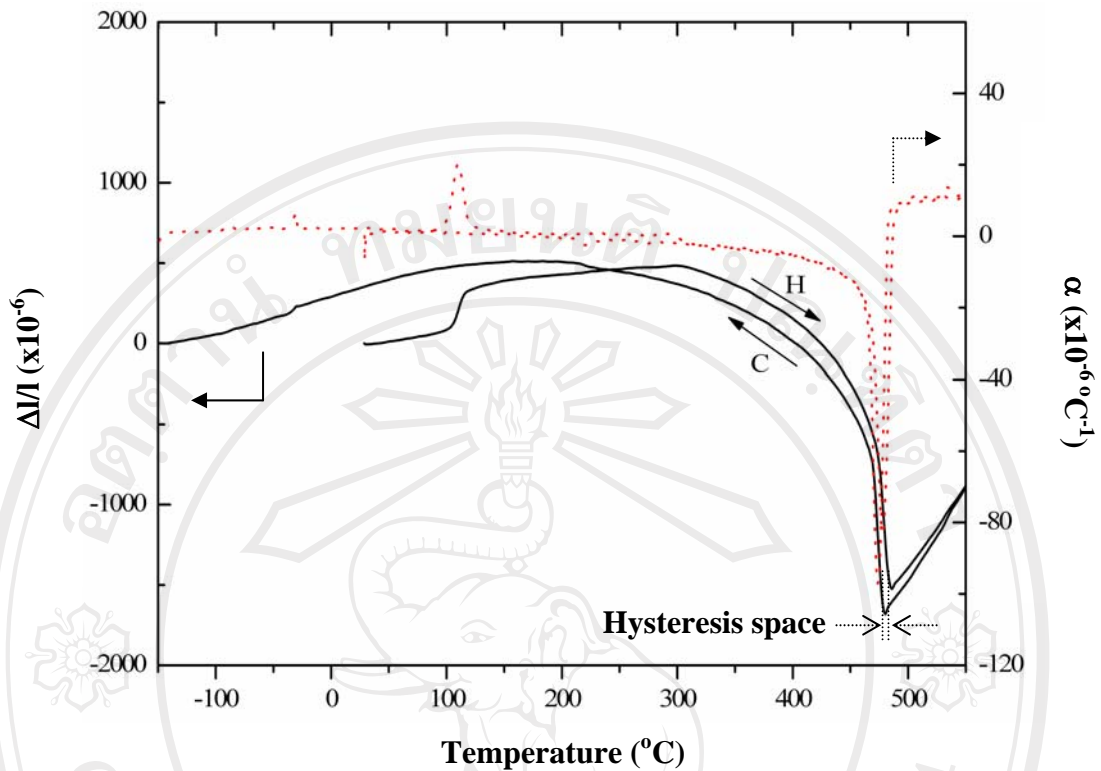


Fig. 5.16 Thermal expansion ($\Delta l/l$) and thermal expansion coefficient (α) of unpoled PT ceramic sintered by two stage process at 900/1200 °C as a function of temperature (H = heating cycle and C = cooling cycle).

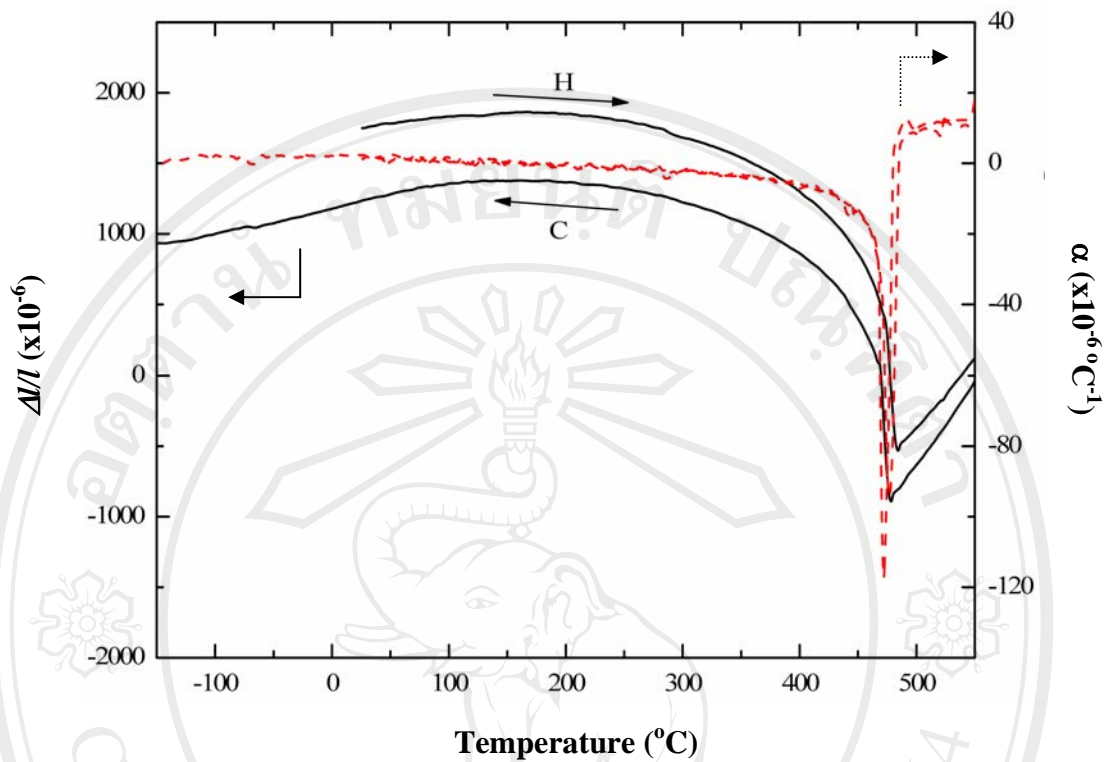


Fig. 5.17 Thermal expansion (along the length direction) as a function of temperature for PT ceramic poled at 30 kV/cm and parallel to the length direction (H = heating cycle and C = cooling cycle).

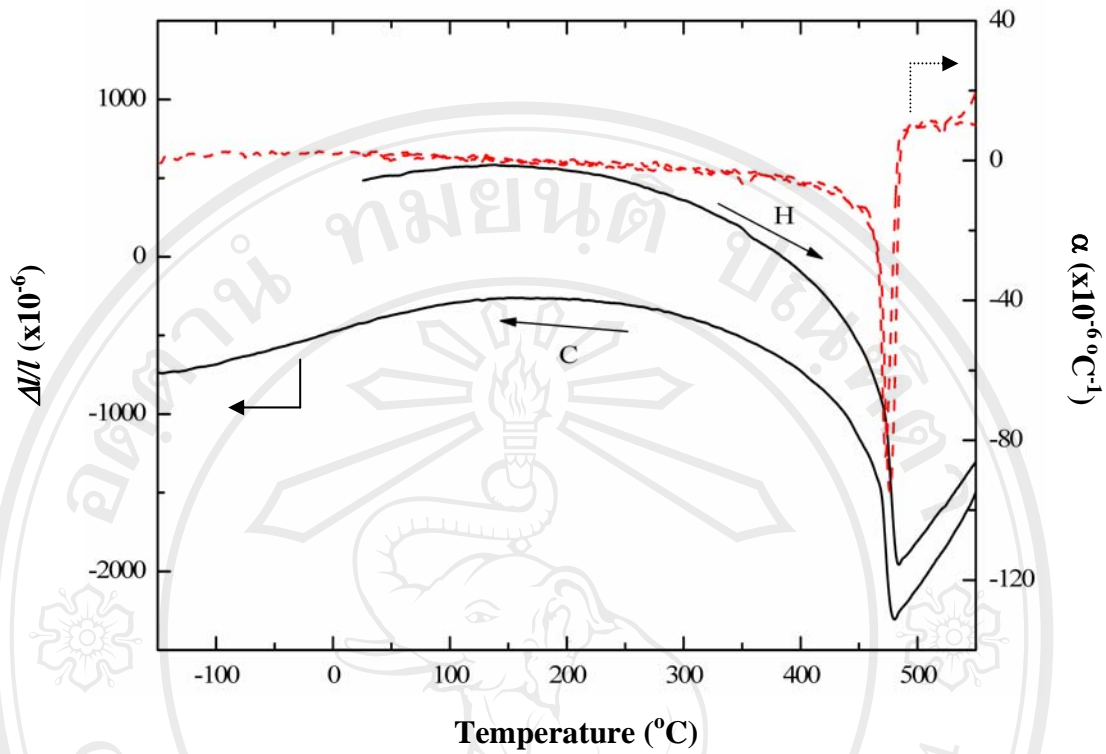


Fig. 5.18 Thermal expansion (along the length direction) as a function of temperature for PT ceramic poled at 45 kV/cm and perpendicular to the length direction (H = heating cycle and C = cooling cycle).

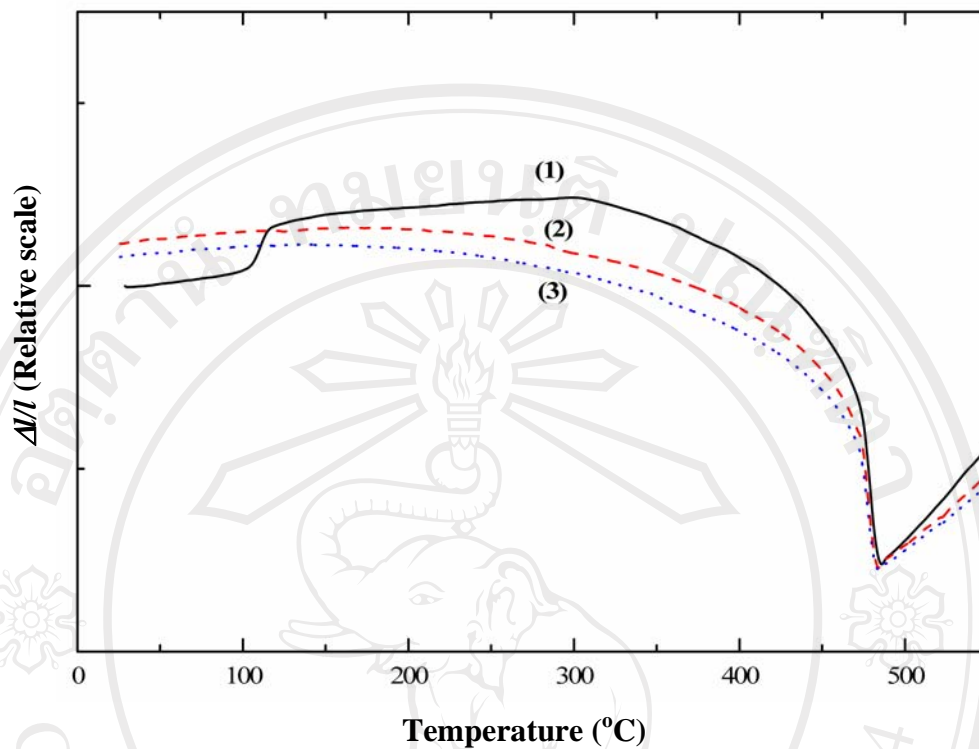


Fig. 5.19 Thermal expansion as a function of temperature for PT ceramics (sample 900/1200 °C) and of different poling states: (1) unpoled, (2) poled parallel to the length direction and (3) poled perpendicular to the length direction, (measurements in heating cycles).

It is always a challenge to measure the temperature-dependence of the polarization of the high T_C ferroelectric over the entire temperature range. In general with the increase in temperature and due to the increase in losses in the PT samples it hinders the real spontaneous polarization and its (P_S) temperature dependence measurements at higher temperature by using the hysteresis and pyroelectric techniques. Therefore, some alternate approaches have to be made in order to extract some useful data on PT for the polarization versus temperature behavior. From the

phenomenological approach we know that the P_S values can be extracted by using Eq. (3.8).

Also, by knowing the $\Delta l/l$ and its temperature dependence, P_S versus temperature as well as the transition temperature of PT and the nature of the transition can be studied. The values of polarization at various temperatures have been computed and can be obtained at various temperatures. Using the values of $Q_{11} = 8.9 \times 10^{-2} \text{ m}^4/\text{C}^2$ and $Q_{12} = -2.6 \times 10^{-2} \text{ m}^4/\text{C}^2$ [181], measurements have also been performed on the unpoled, poled and depoled samples and compared. As clear from the Eq. (3.8) that $\Delta l/l$ is directly related to the square of polarization and thus the measurements do not specifically require the poled samples.

Table 5.5 summarizes the various important features of these measurements. In Fig. 5.20 (a-c) are shown the $P_S = \sqrt{P_S^2}$ values calculated from the thermal expansion data. The agreement in the P_S values is excellent. The values are also in good agreement not only in magnitude but also in the T_C values with the earlier reported results [179,180]. Fig. 5.20 (a), shows the P_S value versus temperature of PT ceramic sintered at 700/1200 °C. The P_S value in the case of unpoled sample is slightly higher than those of both parallel and perpendicular poled samples in temperature range below Curie point, and is caused by the P_S of the poled ceramics.

Also the P_S is smaller than the value in thermally depoled sample. Similar trends have been noticed in the samples sintered under different processing conditions. There are a few factors which could be influencing the measurements. First, there are some sources of contributions to the strain in ferroelectrics, i.e., in addition to the structural component which is present at all temperatures, a component associated with the

appearance of spontaneous polarization in the case of ferroelectric state is also present. The contribution of the spontaneous polarization to strain is due to electrostrictive coupling. Second, after poling it is also possible to have some residual surface charge on the surfaces which can affect the net strain. For perpendicular poling conditions, the net thermal strain might be more along the length due to the positive expansion of a -axis. Therefore, the strain along the length direction can be affected differently in the parallel and perpendicular poled samples. At temperature near T_C , it is seen that the P_S values of both poled samples are sharper compare to those of unpoled and depoled samples. For the other two samples sintered under different conditions, the polarization behaviors are slightly different, however, the magnitude of P_S and trend of polarization behavior are similar to that of 700/1200 °C PT ceramic. The sharpness of the transition increases and the hysteresis space (as shown in Figs. 5.14-5.16) gradually decreases for the samples sintered at higher temperature in first step of the two stage sintering process. It should be noted that because the average grain size of PT ceramic sintered at 700/1200 °C is smaller than those sintered at higher temperatures.

Table 5.5 Summary of the various important features of the thermal expansion measurements for PT ceramics.

Sample (Sintering condition)	T_c (°C)			Calculated P_S at room temperature ($\mu\text{C}/\text{cm}^2$)		
	unpoled	poled	poled \perp	unpoled	poled	poled \perp
1 (700/1200 °C)	489	482	489	74.99	75.76	69.47
2 (800/1200 °C)	481	478	482	75.49	72.28	72.06
3 (900/1200 °C)	478	477	476	76.85	74.62	75.81

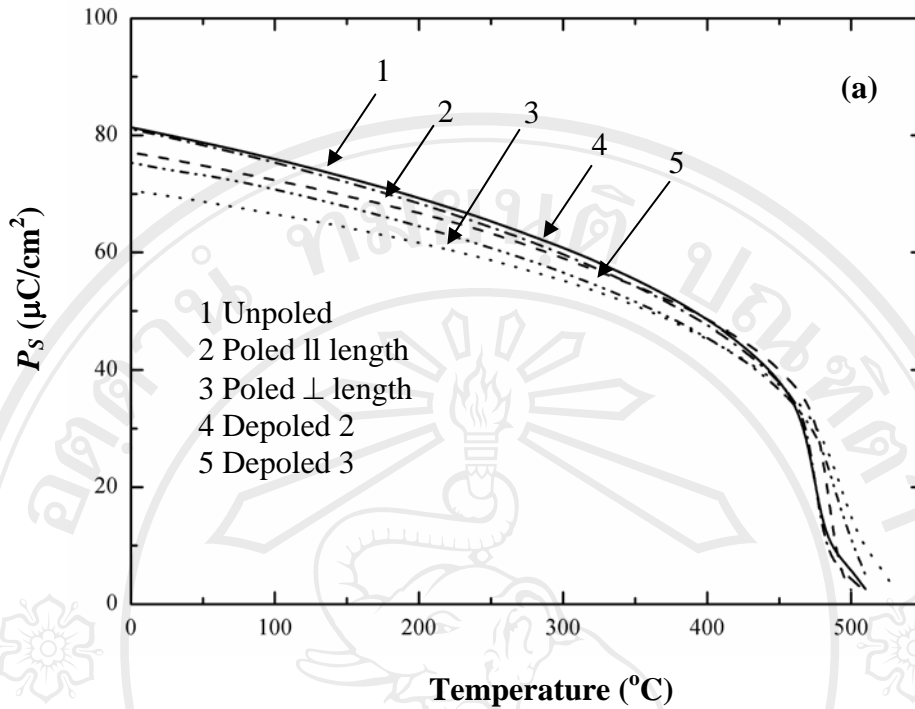


Fig. 5.20 P_S as a function of temperature for PT ceramics with and without poling: (1) unpoled, (2) poled parallel to the length direction, (3) poled perpendicular to the length direction, (4) depoled parallel to the length direction and (5) depoled perpendicular to the length direction; figures a, b, c are for (a) sintered at 700/1200 $^\circ\text{C}$, (b) sintered at 800/1200 $^\circ\text{C}$ and (c) sintered at 900/1200 $^\circ\text{C}$

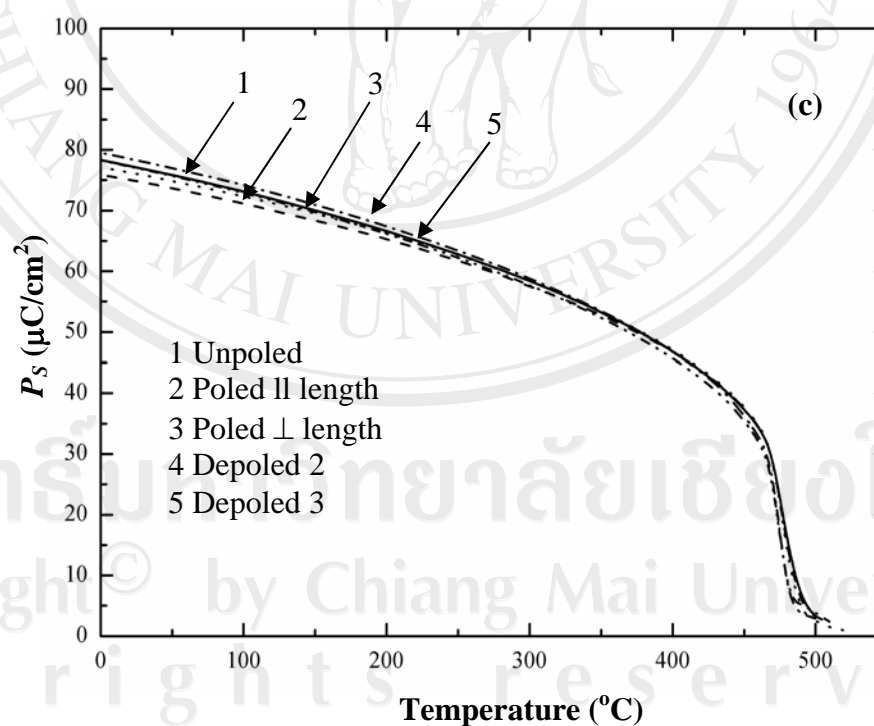
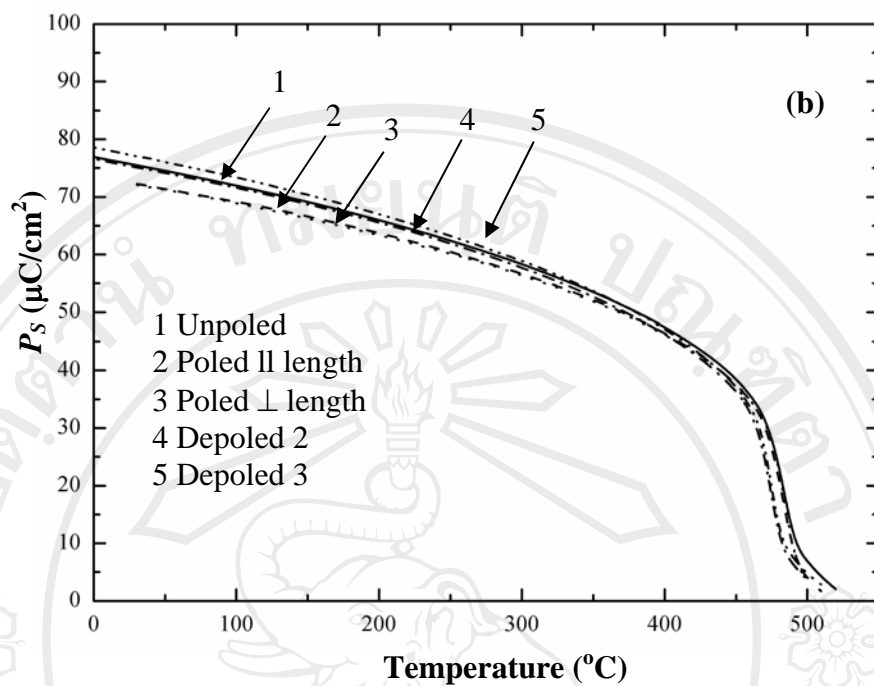


Fig. 5.20 (continued)